Progress In Electromagnetics Research C, Vol. 112, 165–177, 2021

A Dual-Band, Miniaturized, AMC-Based Wearable Antenna for Health Monitoring Applications

Bo Yin, Ming Ye*, Youhai Yu, and Jing Gu

Abstract—A dual-band wearable antenna operating at 2.45 GHz and 5.80 GHz with compact Artificial Magnetic Conductor (AMC) plane is proposed in this paper. The design is based on a U-shaped printed monopole antenna operating in the Industrial, Science, Medical (ISM) bands, and it is integrated with a square looped AMC plane which can reduce the overall size of the antenna system and realize miniaturization. The U-shaped monopole antenna is miniaturized by folding its arms, and its resonant frequency can be tuned easily by adjusting the length of two branches. The AMC unit, which is composed of concentric square double rings, realizes dual-band resonance. Meanwhile, a crossed patch is loaded into the inner ring to increase the electromagnetic coupling and reduce the resonance frequency of the two rings, thus miniaturizing the AMC unit. Therefore, the total size of the AMC plane which contains 3×3 elements is only 59.1 mm $\times$ 59.1 mm. Specific Absorption Rate (SAR) is examined by loading a three-layer human body tissue under the AMC antenna, and the simulation results show that SAR value is only 0.018 W/kg, which is far below the Institute of Electrical and Electronics Engineer (IEEE) standard. Finally, a prototype of the proposed antenna was fabricated and tested, and the experimental results agree well with the simulation responses.

1. INTRODUCTION

Nowadays, with the rapid development of 5G communication technology, Internet of Things is gradually becoming reality. A new type of network named wireless body area network (WBAN), which takes human body as a communication center, is developing and popularizing rapidly. Due to the small size and portability, wearable devices are widely used in WBAN to collect, process, and feed back information. According to the survey, the shipments of smart wearable devices will reach 282 million by 2021, with a total growth rate of 21% in the next four years. Among them, healthy monitoring devices are most expected with which people can manage and improve health more efficiently. Therefore, as a key component of health monitoring device, wearable antenna has a great impact on the overall performance of health testing equipment, which attracts the attention of many researchers.

Wearable antenna was first proposed in a conference paper published by Salonen and Rantanen. In 2001, the authors put forward a dual-band planar inverted-F antenna operating at 900 MHz and 2.4 GHz, but they just advised to reduce the thickness of antenna and initially explored the radiation for human body [1]. In order to integrate the antennas with devices easily, miniaturized antennas were urgently needed. A variety of antenna types, including microstrip patch antenna, inverted-F antenna, monopole antenna, planar and vertical monopole antennas have been widely investigated [2–5]. A 23% miniaturized UWB log-periodic square fractal antenna was achieved by Amini et al., and the fractal geometries of the antenna were designed to add the current length in a limited volume [6]. The increase of path lengths leads to the decrease of resonant frequency and consequently the miniaturization of

Received 22 March 2021, Accepted 28 April 2021, Scheduled 5 May 2021
* Corresponding author: Ming Ye (2057299173@qq.com).
The authors are with the College of Photoelectric Engineering, Chongqing University of Posts and Telecommunications, Chongqing 400065, China.

electrical length of antenna. In the paper, a wideband miniaturized microstrip antenna was documented; a rectangular slot and a cross tuning side were designed in the radiation patch, and the central frequency of UWB antenna can be easily changed by adjusting the length of cross tuning side and rectangular slot [7]. A miniaturized circularly polarized (CP) microstrip antenna was surveyed by Hong et al., in which a spiral structure is applied to miniaturize the CP microstrip antenna. The spiral slot can be equivalent to an inductor, and the resonant frequency can be tuned by adjusting it [8].

Coplanar waveguide (CPW) feeding structure is widely used as the port feeding form of a microstrip antenna due to its advantages such as low radiation loss, small parasitic parameters, and easy connection. A flexible, wide-band antenna was proposed by Hamouda et al. [9]. Li et al. developed a miniaturized, broadband antenna in which symmetrical annular gaps were designed on the radiating surface, and CPW is used for feeding [10].

Different reflection structures such as High Impedance Surfaces (HIS), Electromagnetic Band Gap (EBG), and AMC are designed to isolate the back radiation from the antenna to human body and reduce the SAR value [11–13]. In the study by Ahmad et al., a dual-band EBG was obtained through slotting gaps on a mushroom-liked EBG structure [14]. The backward radiation was suppressed when the EBG structure was loaded. A simple monopole antenna was loaded with an I-shaped AMC at the bottom, and the test results showed that the front to back ratio of the antenna was greatly improved; the backward radiation was effectively suppressed; and it could be bent to a certain extent [15]. Ashyap et al. took textile fabric material as the substrate and loaded an EBG reflector plate at the bottom of the antenna [16]. The overall size of the system was 46 mm × 46 mm × 2.4 mm, and it had the characteristics of miniaturization and high gain.

Dual-band antenna is desirable to improve the communication capacity and efficiency. In addition, in the context of wearable applications, miniaturization design can reduce the space occupied by an antenna while intergrating with other devices efficiently. AMC structure is widely used in the design of low-profile antennas because of its in-phase reflection. In this work, a dual-band AMC wearable antenna is proposed. By folding the monopole arms and coupling between the two arms, the miniaturization and dual bands of the U-shaped monopole antenna are realized. Two U-shaped slots on the metal ground are conducive to the impedance matching of the antenna. The AMC structure adopts an open-ring resonant structure, and the ±90 phase interval of AMC is matched with the two resonant points of the antenna. When the U-shaped monopole antenna is loaded with an AMC structure, its SAR value and radiation performance are observed by the simulation of the antenna system, and the actual performance of the antenna system is measured. It is shown that there is a good agreement between the simulated and measured results. Indicators comparison between this work and reference structures is depicted in Table 4.

2. DESIGN OF ANTENNA AND AMC

2.1. Antenna Design

Due to the special working environment of the wearable antenna, a monopole antenna with a simple radiating structure is proposed in this paper, and coplanar waveguide is used to feed the antenna which can be fabricated on a single-layer substrate. The top view of the proposed antenna structure is shown in Fig. 1. A U-shaped structure is designed to make the antenna work at 2.45 GHz and 5.80 GHz, and the resonance frequency can be tuned by adjusting the length of the branch. The overall size of antenna is 25 mm × 35 mm × 0.15 mm. The proposed antenna is printed on a flexible polyimide film with a dielectric constant of 3.5, a loss tangent of 0.002, and a thickness of 0.15 mm. Table 1 shows the geometrical parameters of the proposed antenna.

By simulating the designed dual-band antenna structure, the reflection coefficient and radiation patterns at different resonant frequencies are obtained, as shown in Fig. 2 and Fig. 3, respectively.

Figure 2 shows that the first band of the proposed antenna is from 2.31 to 2.65 GHz, and the second band covers from 5.67 to 5.97 GHz within which S_{11} is lower than −10 dB. At the point of resonant frequency, the reflection coefficient is lower than −25 dB. Fig. 3 illustrates the simulated radiation patterns of the antenna in free space on the E-plane and H-plane. The shape of the radiation patterns indicates that the antenna has omnidirectional radiation characteristics, and the gain is 2.41 dBi at 2.45 GHz and 3.58 dBi at 5.80 GHz.

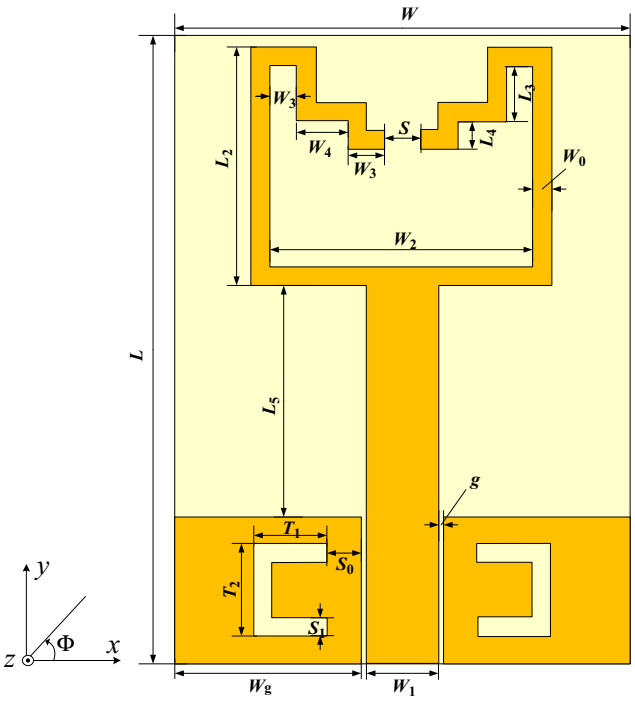

Figure 1. U shaped monopole antenna configuration.

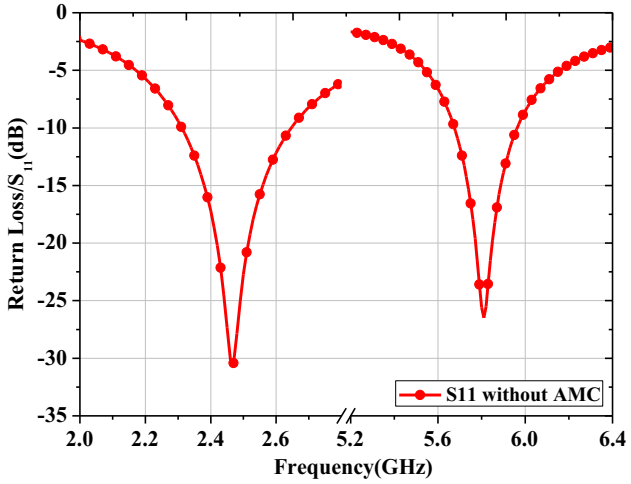

Figure 2. S_{11} of the U shaped monopole antenna without AMC.

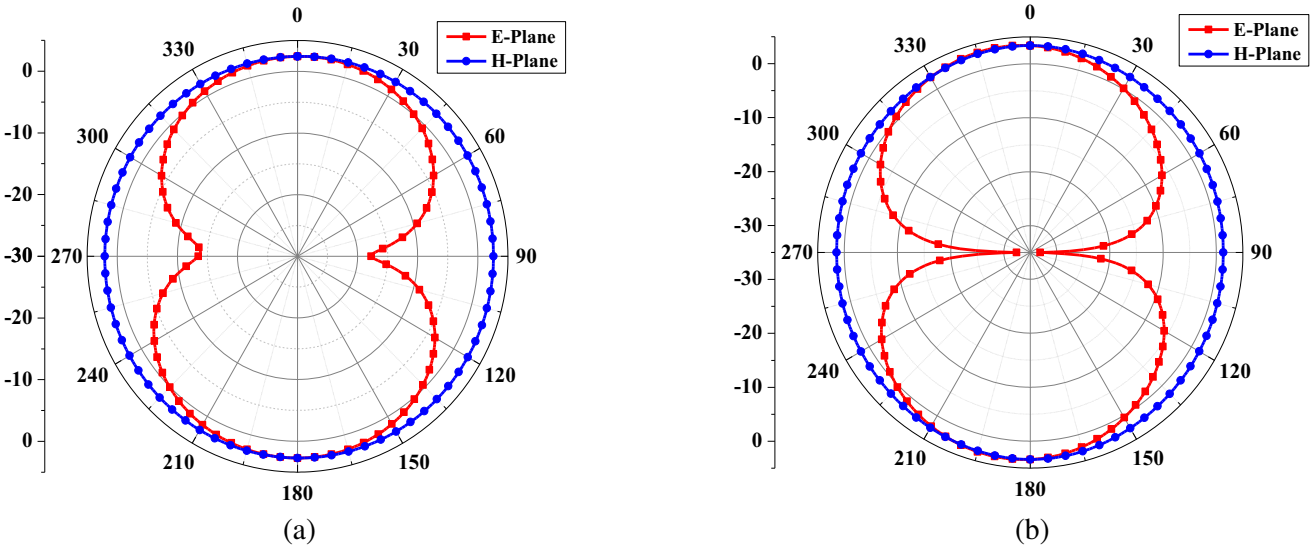

Figure 3. Radiation patterns of the U shaped monopole antenna without AMC at (a) 2.45 GHz and (b) 5.80 GHz.

2.2. AMC Design

According to the electromagnetic (EM) image theory, when the plane EM wave incident to the surface of a Perfect Electric Conductor (PEC), the reflected wave and incident wave will produce a phase shift of 180°, and the EM energy will be cancelled out, which will reduce the radiation efficiency; however, when the plane EM wave incident to the surface of an Perfect Magnetic Conductor (PMC), the phase shift is 0°. In addition, the phase and band gap characteristics of AMC structure will change with the

Table 1. Parameters of the proposed antenna.

Parameter	Value/mm	Parameter	Value/mm	Parameter	Value/mm
W	25	W_4	2.35	S	2
L	35	W_5	2	S_1	1
W_0	1	L_1	8	T_1	4
W_g	10.35	L_2	13.7	T_2	4
W_1	4	L_3	2	g	0.15
W_2	13.7	L_4	1.5	D_1	0.15
W_3	1.5	L_5	13		

frequency of incident wave. Therefore, when the frequency of incident wave and the resonant frequency of AMC structure are the same, the AMC surface can be regarded as a PMC.

In this paper, a square dual-frequency AMC unit cell structure is proposed. Fig. 4(a) shows that the inner ring of the AMC resonates at higher frequency, and the outer ring is responsible for the lower frequency. By changing the size of outer and inner rectangular rings, the resonant frequency can be adjusted. In the center of the inner ring, the cross patch is loaded, which increases the electromagnetic coupling and reduces the resonance frequencies of the inner and outer rings; therefore, the miniaturization of AMC unit is realized. The equivalent circuit model of cell structure, using the transmission line theory, is shown in Fig. 4(b).

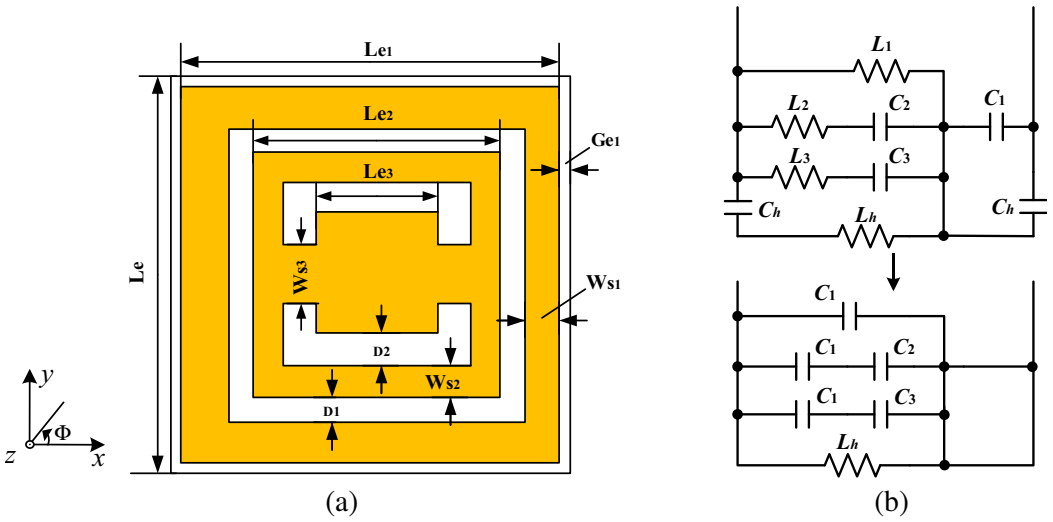

Figure 4. Geometry and equivalent circuit diagram of the AMC unit cell structure. (a) Front view of the AMC unit cell structure. (b) Equivalent circuit diagram of the AMC unit cell structure.

The outer metal ring has small inductance L_1, which can be ignored compared to the serial surface capacitance C_1, caused by the gap between the unit cells. Also, the inner metallic patch has small series inductance L_2, which can be ignored compared to the series capacitance C_2, caused by the gap between the inner and outer rings. Moreover, the central patch has a series inductance L_3, which can be ignored, compared to the series capacitance C_3, caused by gap between the inner ring and central patch. The layers between the AMC patch and ground plane form a capacitance C_h, and the ground plane at the bottom of the AMC cells can be modelled as inductance L_h.

The inductances L_2 and L_3 produced by slotting the AMC surface are negligible, but the values of slotting capacitances C_2 and C_3 would affect the cell's operating performance. The capacitance C_2 caused between inner and outer rings can affect high-frequency characteristics, and capacitance C_1

produced between AMC cells could affect the performance at lower frequency.

The equivalent circuit model can be more simplified by ignoring the small capacitance C_h and inductances L_1, L_2, and L_3. As the structure has dual-band properties, the lower and higher bands can be achieved by analyzing the simplified circuit model [17].

For the lower and higher frequency bands, the impedances Z_L and Z_H are expressed as follows:

$$Z_L = \frac{1}{j\omega C + \dfrac{1}{j\omega L_h}} = \frac{j\omega L_h}{1-\omega^2 L_h C} = \frac{j\omega L_h}{1-\left(\dfrac{\omega}{\omega_L}\right)^2} \tag{1}$$

$$Z_H = \frac{1}{j\omega C_1 + \dfrac{1}{j\omega L_h}} = \frac{j\omega L_h}{1-\omega^2 L_h C_1} = \frac{j\omega L_h}{1-\left(\dfrac{\omega}{\omega_H}\right)^2} \tag{2}$$

where $C = C_1 + C_2 + C_3$, the resonant frequency can be obtained by

$$f_L = \frac{1}{2\pi\sqrt{L_h C}}, \quad f_H = \frac{1}{2\pi\sqrt{L_h C_1}} \tag{3}$$

Following the equations above, the electric parameters can be roughly estimated, and the capacitance produced by gaps between cells or slots of AMC plane has a significant influence on resonant frequencies. When an EM wave is incident on the surface of AMC, it will be reflected in a certain degree, as shown in Fig. 5.

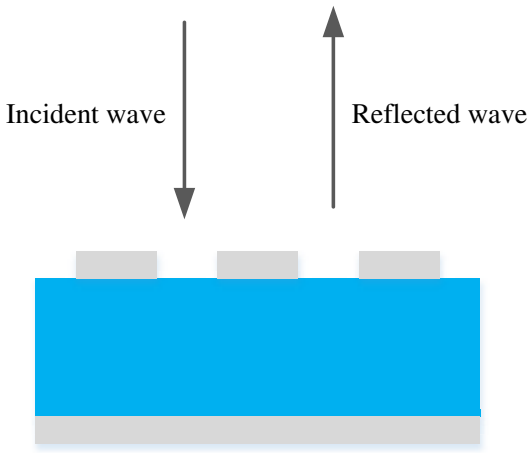

Figure 5. Schematic diagram of incident and reflected waves.

According to the equivalent circuit and classical EM theory, a reflected wave will be generated when an incident wave hits the AMC surface, and the reflection coefficient Γ can be expressed as

$$\Gamma = \frac{\eta - \eta_0}{\eta + \eta_0} = \frac{jX_{LC} - \eta_0}{jX_{LC} + \eta_0} = e^{j\varphi} \tag{4}$$

We define ω_1 and ω_2 as the higher and lower frequencies of EM band gap of AMC. As shown in Eq. (4), when $\eta \gg \eta_0$ and $\omega = \omega_0$, the AMC surface can be equivalent to a perfect magnetic conductor (PMC), and reflected phase $\varphi = 0°$. When $\omega_1 > \omega > \omega_2$ and $X_{LC} < 0$, the AMC can be regarded as an inductive surface, and reflected phase $\varphi < 0°$. When $\omega_2 < \omega < \omega_0$ and $X_{LC} > 0$, the AMC is equivalent to a capacitive surface, and reflected phase $\varphi > 0°$. Here, we use the Floquet method to simulate the reflect phase characteristic of AMC, and the simulated band gap response is shown in Fig. 6.

The length of AMC unit cell is 19.7 mm. The frequency point of zero reflection phase is 5.80 GHz for the former and 2.45 GHz for the latter. The band gaps of two points are 2.40–2.50 GHz and 5.60–5.95 GHz. It is obvious that the former band gap is wider than the latter, and they both cover the ISM band. Table 2 lists the geometrical parameters of AMC. In order to study the effects of different sizes of

Table 2. AMC parameters and dimension.

Parameter	Value/mm	Parameter	Value/mm	Parameter	Value/mm
Le	19.7	$Le3$	6.0	$Ws3$	2.7
$Le1$	18.7	$Ws1$	2.1	$Ge1$	0.5
$Le2$	12.0	$Ws2$	1.5	$d3$	1.5
$D1$	3.75	$D2$	1.5		

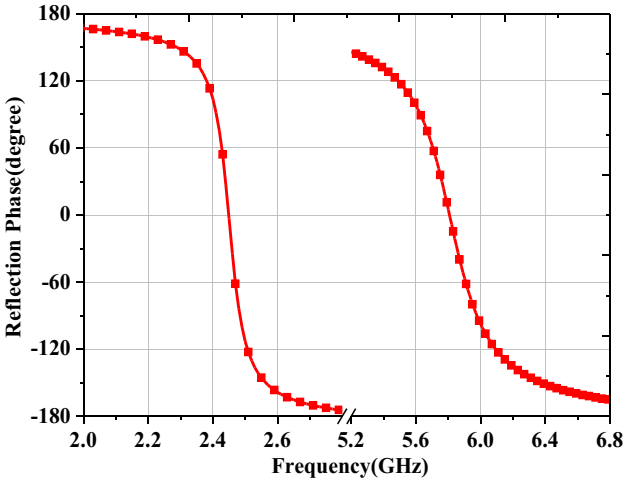

Figure 6. Simulation of reflection phase of AMC unit cell.

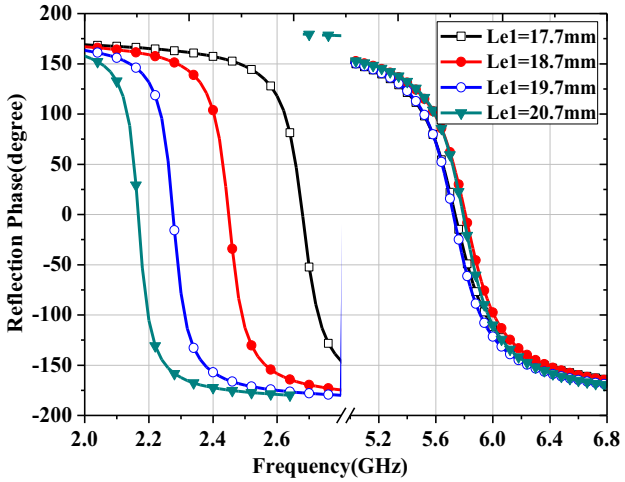

Figure 7. Reflection phases of AMC with different $Le1$.

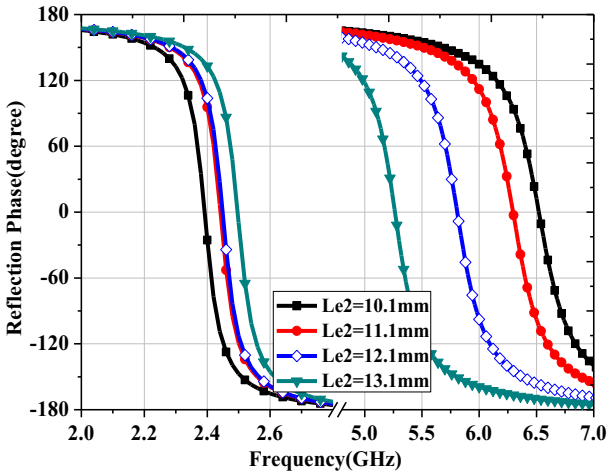

Figure 8. Reflection phases of AMC with different $Le2$.

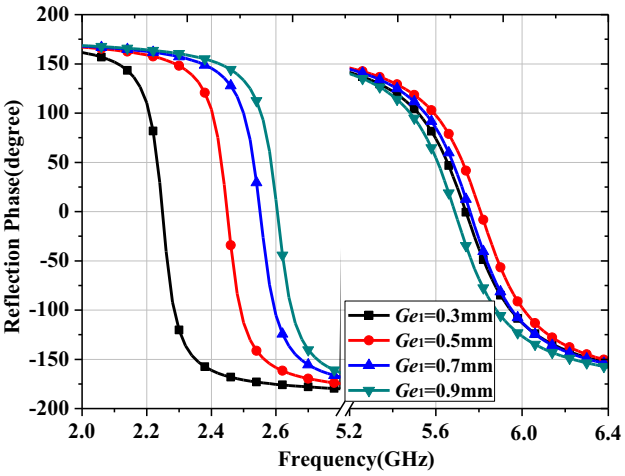

Figure 9. Reflection phases of AMC with different $Ge1$.

cell structure on the reflected phase, we sweep two parameters, $Le1$ and $Le2$, to analyze their influence. Fig. 7 and Fig. 8 depict the comparative results of the different values.

As shown in Fig. 7, with the increase of $Le1$ size, the reflection phase of 0° shifts to low frequency, and the bandgap of ±90° reflection phase becomes narrower. This phenomenon can be explained by the fact that the decrease of $Le1$ leads to larger C_1, and the zero-phase frequency of low band decreases with

the increase of C_1 which is consistent with the characteristics described in Equation (3). The change of $Le1$ mainly affects the reflection phase at low frequency, but has little effect on the phase at high frequency. When $Le1 = 18.7$ mm, the AMC cell structure obtains 0° reflection phase point at 2.45 GHz.

The change of $Le2$ has an effect on the reflection phase at low and high frequencies, but the effect is more obvious at high frequencies as shown in Fig. 8. When $Le2$ is increased, which can be equivalent to the increase of C_2, the zero-phase frequency in high band decreases. The larger the $Le2$ is, the more the reflection phase points at high frequencies shift to low frequencies, which is consistent with the law described in Equation (3). When $Le2 = 12.1$ mm, the reflection phase points at 5.80 GHz are obtained for AMC cell structure.

The gap between two adjacent AMC units mainly affects the reflection phase at low frequency, as shown in Fig. 9. With the increase of $Ge1$, the reflection phase point at 0° shifts to high frequency, which can completely cover 2.4–2.5 GHz of ISM low frequency band. The effect of $Ge1$ on the reflection phase at high frequencies is relatively small. Considering that the ±90° reflection phase band gap of the designed AMC cell structure should cover low and high frequencies at the same time, $Ge1 = 0.5$ mm is chosen, that is, the gap width between two adjacent AMC cells is 1 mm.

3. WEARABLE ANTENNA SYSTEM BASED ON AMC

3.1. Antenna with AMC Structure

The AMC units are arranged into a 3×3 array to form a plane, which is used as the reflector of the antenna. Then the antenna is placed 2.5 mm above the AMC reflector, as shown in Fig. 10. The overall size of the dual-band structure is 59.1×59.1 mm^2 with a height of 4.1 mm. The reflective coefficients and radiation patterns of the system are given in Fig. 11 and Fig. 12, respectively.

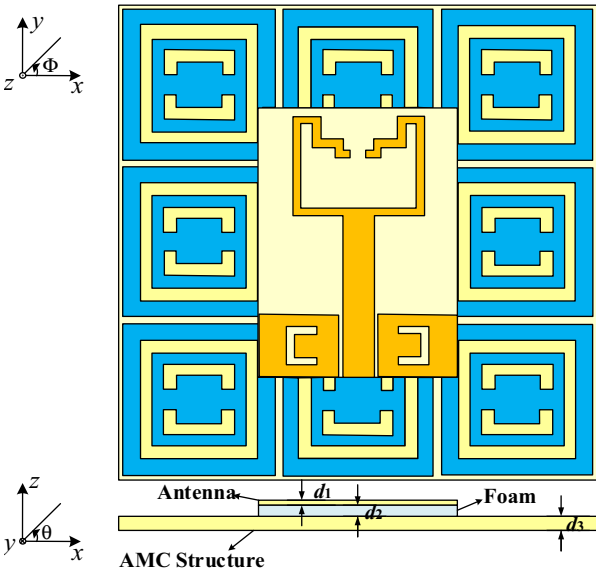

Figure 10. Dual-band antenna with AMC.

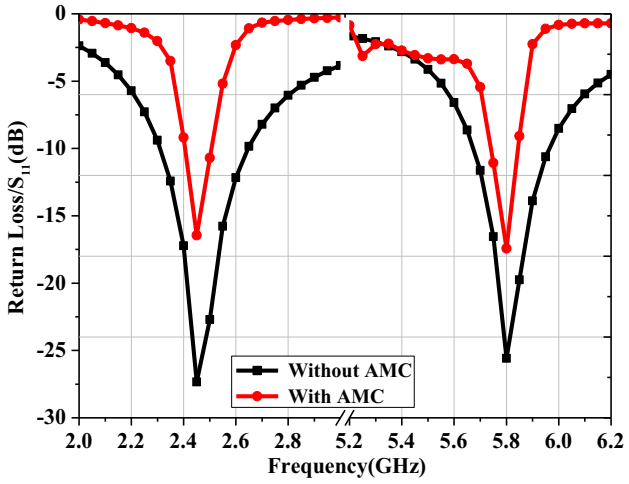

Figure 11. $|S_{11}|$ of antenna with and without AMC.

The simulation results show that the monopole antenna still has dual-band resonant frequencies when loading the miniaturized AMC structure. The antenna system works at 2.45 GHz and 5.80 GHz of the ISM band, and the value of S_{11} at low resonant point reaches −16.46 dB and −17.43 dB at high one. Limited by ±90° reflection phase band gap of the designed AMC, the operation bandwidth of the antenna system loaded with AMC is narrower than before, and the −10 dB bandwidth covers 2.41–2.51 GHz and 5.72–5.85 GHz, respectively, which satisfies the requirement of a wearable antenna in ISM band.

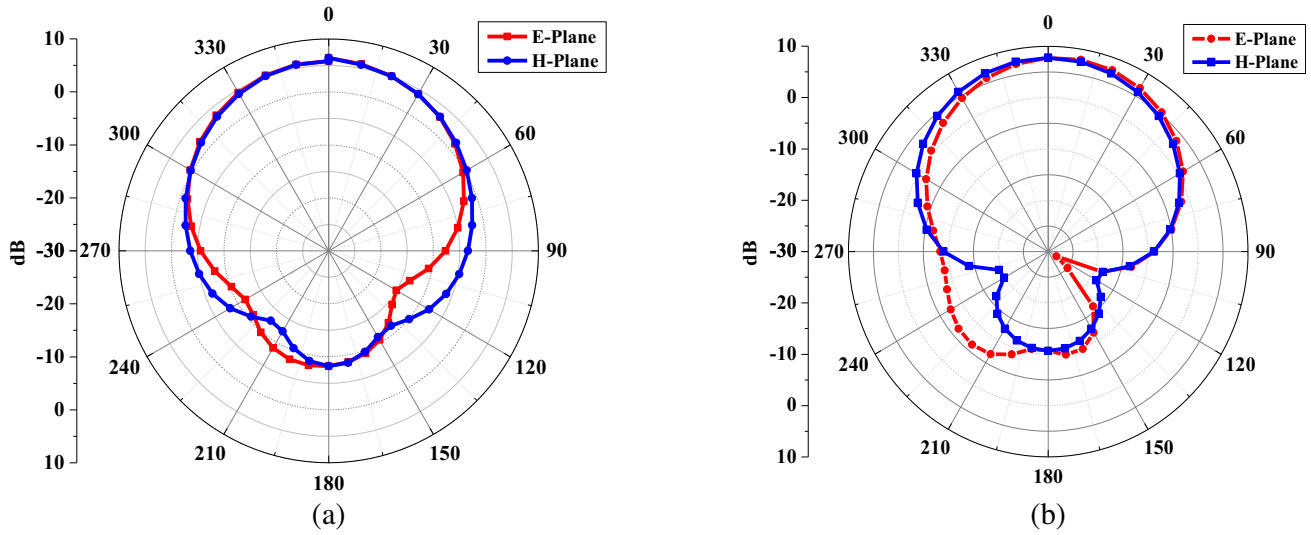

Figure 12. Simulated radiation patterns with AMC at (a) 2.45 GHz, (b) 5.80 GHz.

It is evident from Fig. 12 that a considerable improvement in terms of gain is achieved (4 dBi) by including the AMC structure. The simulated gain for the proposed antenna system is 6.43 dBi at 2.45 GHz and 7.75 dBi at 5.80 GHz. An increase in the simulated front to back ratio around 20 dB is achieved. The front to back ratio can be further improved if we use a wider AMC unit cell. However, this solution would enlarge the system.

3.2. SAR Evaluation

In addition, part of the electromagnetic waves radiated by the antenna will be absorbed by human tissues, and the electromagnetic waves absorbed can resonate with human molecules and generate thermal effects. In 1990, IEEE set standards for electromagnetic radiation. Specific Absorption Rate (SAR) was used to evaluate the electromagnetic power deposition in human tissues. SAR value must not exceed the limit of 1.67 W/kg averaged over 1 g and 2 W/kg averaged over 10 g of human tissues. The following equation relates SAR with the applied input power:

$$\mathrm{SAR} = \frac{\sigma |E^2|}{\rho} \tag{5}$$

where σ represents the conductivity of the tissue in S/m, E the electric field intensity in V/m, and ρ the mass density of the tissue in kg/m^3. The signal power is often set as 1 W in HFSS when simulations are conducted, and the relationship between the signal power density and electric field intensity is:

$$\mathrm{Power}\,(\mathrm{W/m^2}) = (E\,(\mathrm{V/m}))^2/377 \tag{6}$$

In order to simulate the SAR value of the designed antenna system working on the surface of human body, a three-layer tissue model that is close to the actual electrical parameters of the human body consisting of skin, fat, and muscle is constructed in Fig. 13. The antenna is placed on the tissue model surface for simulation. The electrical parameters of the constructed human body model are listed in Table 3, and the result is shown in Fig. 14.

Figure 14 shows that the SAR value of antenna with AMC is close to 0.018 W/kg at 2.45 GHz and 0.015 W/kg at 5.8 GHz when the measuring distance is longer than 3 mm, which is far below the standard defined by IEEE. In order to observe the electric field inside the human tissue, a YZ plane vertical to the antenna plane is established, and the distribution of electric field across the tissue on YZ plane is shown in Fig. 15. We can observe from Fig. 15 that the main radiating EM wave absorbed by tissue is from the edge of the AMC structure. The reference line, which is used to simulate the SAR, is set in the central below the AMC plane so that the SAR value will be nearly a constant as a function of tissue depth.

Table 3. The electric parameters of the human tissues.

Frequency	Skin		Fat		Muscle	
	ε_r	tan	ε_r	tan	ε_r	tan
2.45 GHz	38.007	0.295	5.280	0.145	52.729	0.245
5.8 GHz	35.114	0.334	4.955	0.126	48.485	0.323

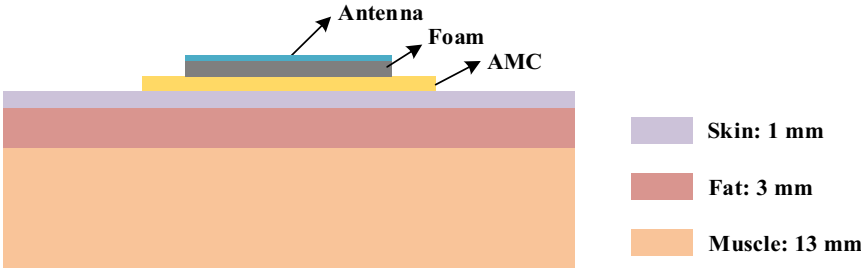

Figure 13. Model of AMC antenna system with human tissues.

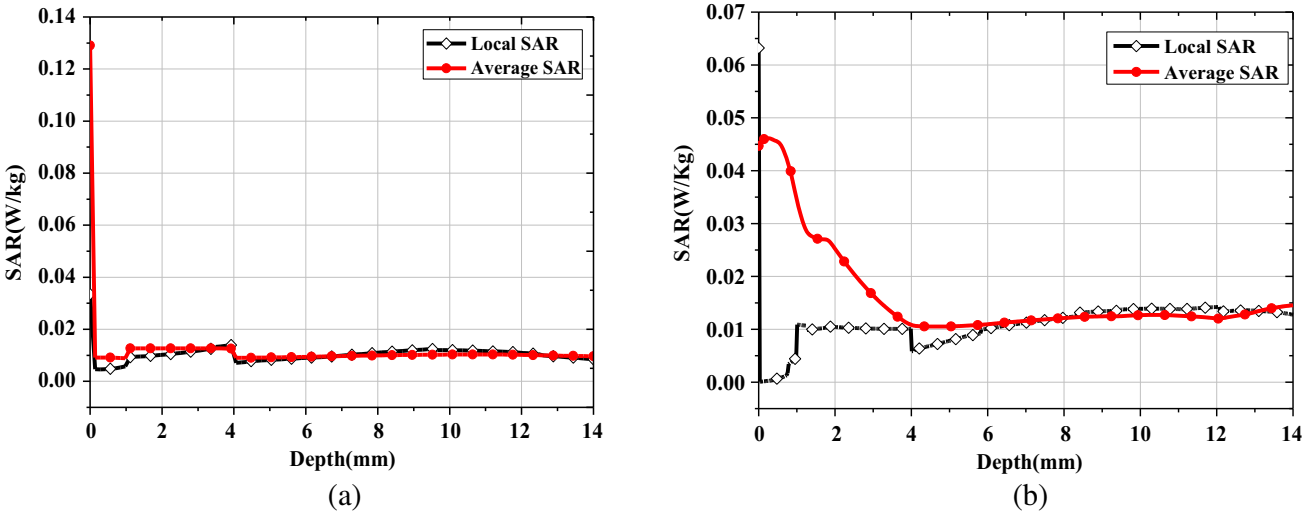

Figure 14. Simulated SAR of antenna system on body at (a) 2.45 GHz, (b) 5.8 GHz.

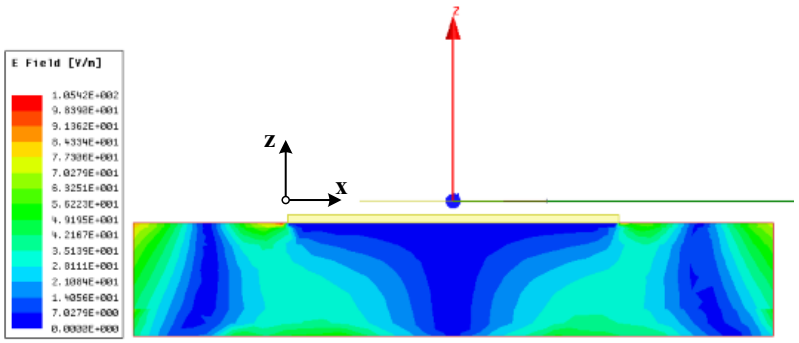

Figure 15. Distribution of electric fields across the tissue on YZ plane.

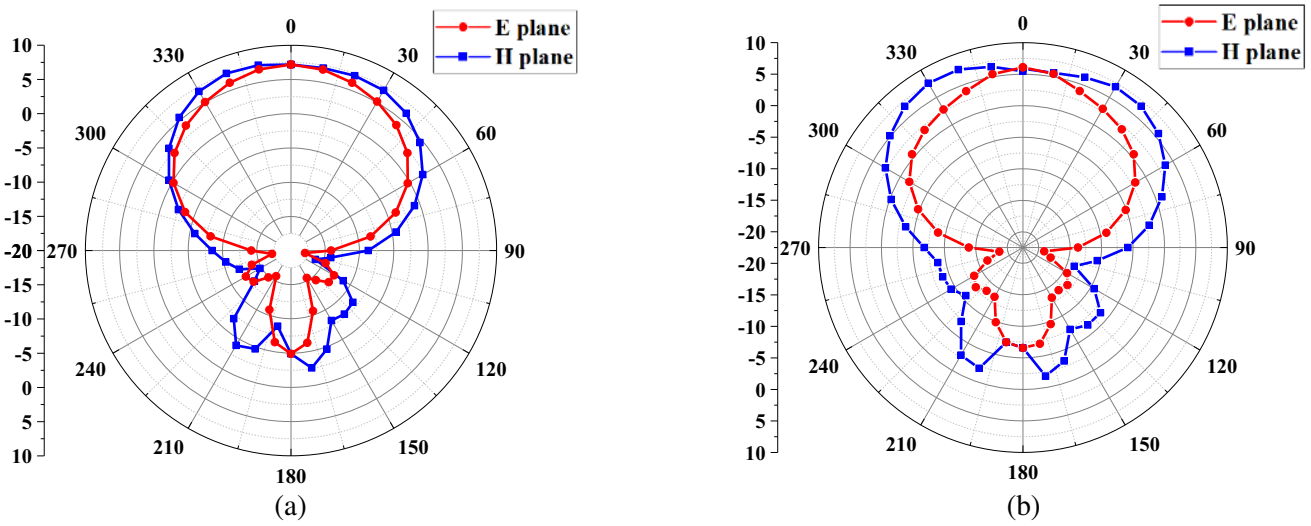

Figure 16. Simulated radiation patterns with human tissues at (a) 2.45 GHz and (b) 5.8 GHz.

It can be conducted from Fig. 16 that the backward radiation EM wave is more concentrated when the human tissue is loaded under AMC antenna, and the axial gains at two resonant frequencies have slight decrease with 0.51 dBi and 0.96 dBi at 2.45 GHz and 5.80 GHz, respectively, compared to Fig. 12 which indicates the radiation patterns of AMC antenna without human tissues, and the gain's reduction may be due to the absorption of the EM wave by human tissues.

4. FABRICATION AND TEST

The proposed antenna system is manufactured as shown in Fig. 17. The antenna is placed 1.5 mm above the AMC reflector, and foam is used to fill the gap. A 15 cm radio frequency cable is used to extend the current path and feed the antenna. A piece of transparent tape is fixed on the back of the AMC reflector, and the antenna system is suspended on the chest of a male human body with a height of 176 cm and weight of 65 kg in Fig. 18. The AMC antenna system is measured by the Keysight PNA37 Network analyzer. Fig. 19 shows the simulated and measured reflection coefficients.

Figure 19 shows that there is a relatively good agreement between the simulated and measured results when the antenna system is operated on human body. Both resonant frequencies of the AMC

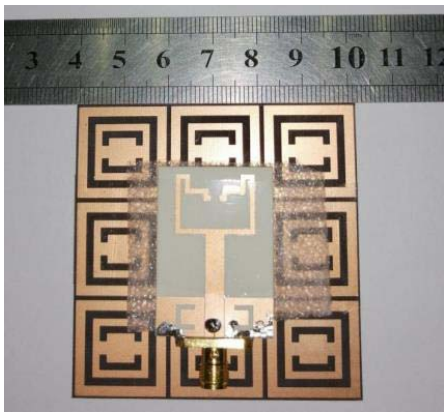

Figure 17. The top view of the fabricated antenna with AMC.

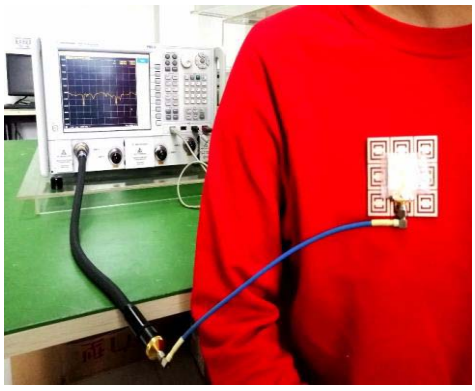

Figure 18. Measured photograph of the fabricated antenna placed on the human body.

antenna have slight shift, but the −10 dB bandwidth still basically covers the required band. A subtle deterioration in the non-resonant frequency band can be observed, and it may be caused by fabrication and finite number of AMC cells. At 5.8 GHz, S_{11} has a difference of about −5 dB, which may be caused by the antenna fabrication and the SMA joint welding during the test.

In order to observe the far-field radiation patterns, the proposed antenna was put inside an anechoic chamber in Chong Qing University of Post and Telecommunications, the measuring setup is shown in Fig. 20. Fig. 21 depicts the simulated and measured radiation patterns of AMC antenna operating at 2.45 GHz and 5.80 GHz.

The measured results show that the gain of AMC antenna was enhanced from 2.41 dBi to 6.43 dBi at 2.45 GHz and 3.58 dBi to 6.85 dBi at 5.80 GHz, and the radiation gain is about 4 dBi higher than that of a single monopole antenna. However, there is still a little discrepancy between the simulated and measured results, which is probably contributed by the fabrication tolerance and measuring environment.

Moreover, comparisons among the proposed antenna and reported antennas operating at lower frequency (2.45 GHz) are listed in Table 4, which indicates that the proposed AMC antenna has a smaller size than those in references, and the SAR value is far below the IEEE standard.

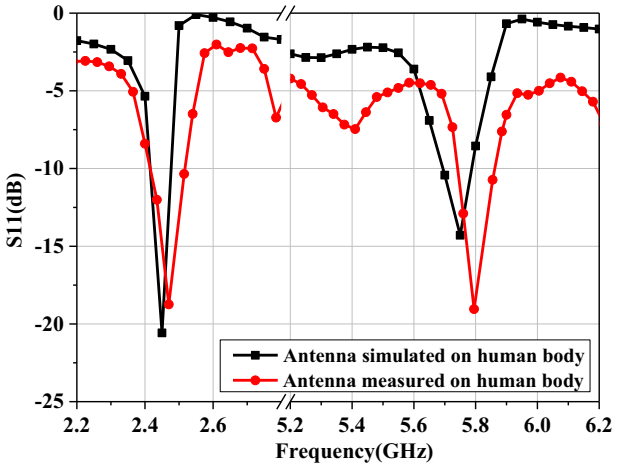

Figure 19. Simulated and measured S_{11} of AMC antenna system on human body.

Figure 20. Photograph of far-field radiation pattern testing in an anechoic chamber.

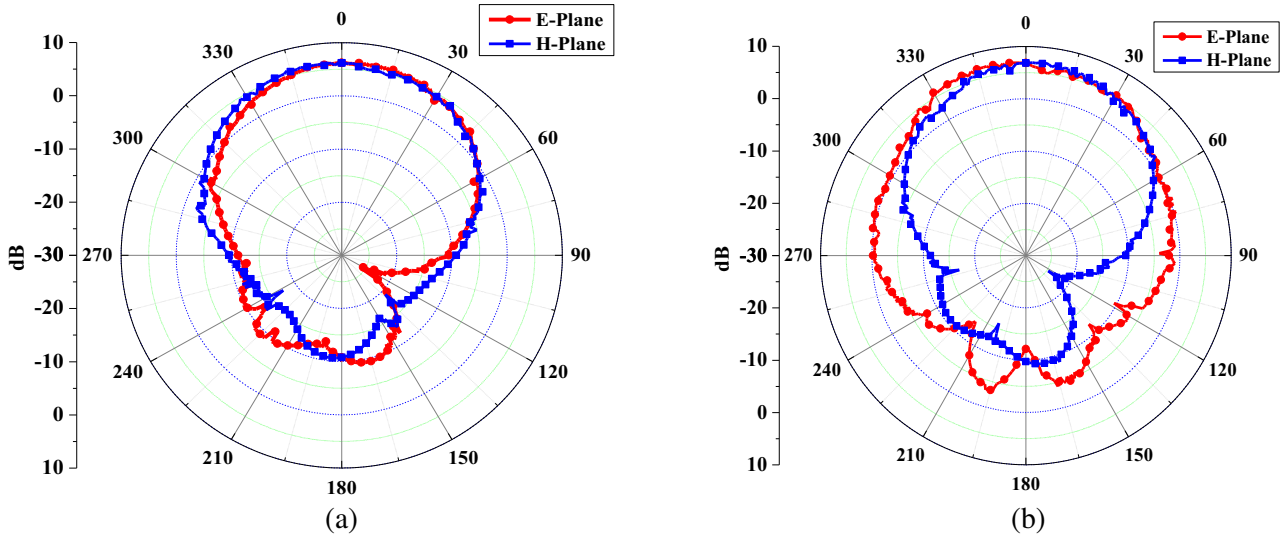

Figure 21. Measured radiation patterns of the fabricated antenna on body at (a) 2.45 GHz and (b) 5.80 GHz.

Table 4. Comparison of the proposed antenna and references.

Ref	Freq/GHz	Gain/dBi	Number of cells	Dimension/mm^3	SAR (W/kg)/10 g	Reflected plane
[18]	1.80/2.45	2.2/2.5	3×3	$150 \times 150 \times 3.5$	0.024/0.016	EBG
[19]	2.45/5.8	N/A	3×3	$120 \times 120 \times 4.3$	0.043/0.090	EBG
[20]	2.45	0.95	4×3	$150 \times 120 \times 3.1$	N/A	EBG
[21]	2.45/5.8	2.5/3.0	4×4	$100 \times 100 \times 1.5$	0.046/0.030	AMC
[22]	1.8/5.5	3.49/7.66	3×3	$70 \times 70 \times 3.5$	0.841/0.647	EBG
This paper	2.45/5.8	6.43/6.85	3×3	$59.1 \times 59.1 \times 4.15$	0.018/0.016	AMC

5. CONCLUSION

A miniaturized dual-band wearable antenna with an AMC structure for WBAN is proposed in this paper. Table 4 provides comparisons among the proposed antenna and structures published in reference papers. The proposed antenna covers the ISM band at 2.45 GHz and 5.80 GHz, and it has an overall size of 59.1 mm $\times$ 59.1 mm which is smaller than antenna sizes in the references. A U-shaped monopole antenna is selected as the primary radiator, and the resonant frequency can be adjusted through changing the length of branch. A 3×3 array of rectangular and circular AMC reflectors was applied to enhance the gain and reduce the backward radiation of the antenna; the dimension of the unit cell is just 0.16λ (at 2.45 GHz). The measured results are basically consistent with the simulation ones, and a significant increase in gain is noted for the proposed antenna compared with the reference structures for 6.43 dBi at 2.45 GHz and 6.85 dBi at 5.80 GHz. A three-layer human tissue model is established to evaluate the SAR, and the simulated results show that the AMC plane can isolate much of the back radiation from the antenna to human body with a SAR value of 0.018 W/kg, far below the IEEE standard. All above make the antenna suitable for health medical applications.

ACKNOWLEDGMENT

This work was supported by the National Natural Science Foundation of China (61601074 and 41606203), Chongqing Technology Innovation and Application Development Project (cstc2019jscx-msxmX0079) and the Chongqing Basic Science and Frontier Technology Research Project (cstc2017jcyjAX0193 and cztc2018jcyjAX0508).

REFERENCES

1. Salonen, P. and J. Rantanen, "A dual-band and wide-band antenna on flexible substrate for smart clothing," *27th Annual Conference of the IEEE Industrial Electronics Society, IECON'01*, 125–130, 2001.
2. Gao, G., C. Yang, B. Hu, R. Zhang, and S. Wang, "A wide-bandwidth wearable all-textile PIFA with dual resonance modes for 5 GHz WLAN applications," *IEEE Trans. Antennas Propag.*, Vol. 67, No. 6, 4206–4211, Mar. 2019.
3. Wang, F. and T. Arslan, "A wearable ultra-wideband monopole antenna with flexible artificial magnetic conductor," *Loughborough Antennas & Propagation Conference, LAPC*, 1–5, 2016.
4. Atanasov, N. T., G. L. Atanasova, A. K. Stefanov, and I. I. Nedialkov, "A wearable, low-profile, fractal monopole antenna integrated with a reflector for enhancing antenna performance and SAR reduction," *IEEE MTT-S International Microwave Workshop Series on Advanced Materials and Processes for RF and THz Applications, IMWS-AMP*, 67–69, 2019.

5. Asif, S. M., A. Iftikhar, B. D. Braaten, D. L. Ewert, and K. Maile, "A wide-band tissue numerical model for deeply implantable antennas for RF-powered leadless pacemakers," *IEEE Access*, Vol. 7, 31031–31042, 2019.
6. Amini, A., H. Oraizi, and M. A. Chaychizadeh, "Miniaturized UWB log-periodic square fractal antenna," *IEEE Antennas and Wireless Propagation Letters*, Vol. 14, 1322–1325, Mar. 2015.
7. Deng, D., L. Wang, Z. Luo, B. Yan, L. Feng, and H. Zheng, "Design of miniaturized WLAN notched ultra-wideband microstrip antenna," *International Symposium on Antennas, Propagation and EM Theory, ISAPE*, 291–294, 2016.
8. Hong, T., S. Gong, Y. Liu, W. Jiang, and J. Du, "Miniaturized circularly polarized microstrip antenna by spirally slotted," *IEEE 4th Asia-Pacific Conference on Antennas and Propagation, APCAP*, 585–586, 2015.
9. Hamouda, Z., J. Wojkiewicz, A. A. Pud, L. Koné, S. Bergheul, and T. Lasri, "Magnetodielectric nanocomposite polymer-based dual-band flexible antenna for wearable applications," *IEEE Trans. Antennas Propag.*, Vol. 66, No. 7, 3271–3277, Jul. 2018.
10. Li, X., Y. C. Jiao, and Z. Li, "Wideband low-profile CPW-fed slot-loop antenna using an artificial magnetic conductor," *Electronics Letters*, Vol. 54, No. 11, 673–674, May 2018.
11. Mersani, A., L. Osman, and J. M. Ribero, "Performance of dual-band AMC antenna for wireless local area network applications," *IET Microwaves Antennas and Propagation*, Vol. 12, No. 6, 872–878, May 2018.
12. Lin, M., Y. Huang, and C. G. Hsu, "Design a dual-band high-impedance surface structure for electromagnetic protection in WLAN applications," *International Symposium on Electromagnetic Compatibility*, 525–528, 2014.
13. Wang, M. J., Z. Yang, J. F. Wu, et al., "Investigation of SAR reduction using flexible antenna with metamaterial structure in wireless body area network," *IEEE Trans. Antennas Propag.*, Vol. 66, No. 6, Jun. 2018.
14. Ahmad, A., F. Faisal, S. Khan, S. Ullah, and U. Ali, "Performance analysis of a wearable and dual band planar antenna using a mushroom-like electromagnetic bandgap (EBG) ground plane," *International Conference on Open Source Systems & Technologies, ICOSST*, 24–29, 2015.
15. Jiang, Z. H., D. E. Brocker, P. E. Sieber, and D. H. Werner, "A compact, low-profile metasurface-enabled antenna for wearable medical body-area network devices," *IEEE Trans. Antennas Propag.*, Vol. 62, No. 8, Aug. 2014.
16. Ashyap, A. Y. I., Z. Z. Abidin, S. H. Dahlan, et al., "Compact and low-profile textile EBG-based antenna for wearable medical applications," *IEEE Antennas and Wireless Propagation Letters*, Vol. 16, 2550–2553, Jul. 2017.
17. Yading, L., K. Esselle, A. Weily, and Y. Ge, "A dual-band planar compact artificial magnetic conductor," *IEEE Antennas and Propagation Society International Symposium*, 451–454, 2005.
18. Velan, S., E. F. Sundarsingh, A. K. Sarma, et al., "Dual-band EBG integrated monopole antenna deploying fractal geometry for wearable applications," *IEEE Antennas and Wireless Propagation Letters*, Vol. 14, 249–252, Sep. 2015.
19. Zhu, S. and R. Langley, "Dual-band wearable textile antenna on an EBG substrate," *IEEE Trans. Antennas Propag.*, Vol. 57, No. 4, Apr. 2009.
20. Kim, S., Y. Ren, H. Lee, A. Rida, S. Nikolaou, and M. M. Tentzeris, "Monopole antenna with inkjet-printed EBG array on paper substrate for wearable applications," *IEEE Antennas and Wireless Propagation Letters*, Vol. 11, 663–666, Jun. 2012.
21. Yan, S., P. J. Soh, and G. A. E. Vandenbosch, "Low-profile dual-band textile antenna with artificial magnetic conductor plane," *IEEE Trans. Antennas Propag.*, Vol. 62, No. 12, Dec. 2014.
22. Abdu, A., H. X. Zheng, J. H. Adamu, and M. J. Wang, "CPW-fed flexible monopole antenna with H and two concentric C slots on textile substrate, backed by EBG for WBAN," *International Journal of RF and Microwave Computer-Aided Engineering*, Vol. 28, No. 7, Sep. 2018.